

Review

# Spectroscopic Chemical Sensing and Imaging: From Plants to Animals and Humans

Pietro Strobbia <sup>1,2</sup> , Ren A. Odion <sup>1,2</sup> and Tuan Vo-Dinh <sup>1,2,3,\*</sup>

<sup>1</sup> Fitzpatrick Institute for Photonics, Duke University, Durham, NC 27708, USA; ps228@duke.edu (P.S.); ren.odion@duke.edu (R.A.O.)

<sup>2</sup> Department of Biomedical Engineering, Duke University, Durham, NC 27708, USA

<sup>3</sup> Department of Chemistry, Duke University, Durham, NC 27708, USA

\* Correspondence: tuan.vodinh@duke.edu

Received: 15 January 2018; Accepted: 20 February 2018; Published: 26 February 2018

**Abstract:** Chemical sensing and imaging technologies are of great importance in medical diagnostics and environmental sensing due to their ability to detect and localize chemical targets and provide valuable information in real-time. Biophotonic techniques are the most promising for *in vivo* applications due to their minimal invasivity. Our laboratory has introduced various biophotonics-based technologies for chemical sensing and imaging for biochemical sensing, medical diagnostics, and fundamental research. Over the years, we have developed a wide variety of fluorescence and surface-enhanced Raman scattering (SERS)-based technologies for the detection of biomarkers for cancer and other diseases. This paper provides an overview of the research on chemical and biological sensors developed in our laboratory, highlighting our work on *in vivo* imaging and sensing, including minimally invasive detection of endogenous fluorophores associated with malignant tissue, SERS-tag localization of cancer cells and tissues, and SERS-based detection of nucleic acid biotargets and its feasibility for *in vivo* applications. This manuscript also presents new development on the use of Raman imaging of SERS-labeled nanoprobe incubated in leaves for use in biofuel research, laying the foundation for studies on functional imaging of nucleic acid biomarkers in plants.

**Keywords:** sensor; imaging; fluorescence; Raman; surface-enhanced Raman scattering (SERS); plasmonics; nanotechnology

## 1. Introduction

The ultimate goal of chemical sensing and imaging technologies is to detect and localize chemical targets *in vivo* and provide valuable information in real-time. These technologies are of key importance in many areas ranging from environmental sensing and bioenergy system monitoring to medical imaging and diagnostics. Chemical sensing and imaging provides an additional layer of information over widely used physical imaging techniques (e.g., magnetic resonance and X-ray transmission) by providing the concentration and location of a specific chemical component, which that can be associated with a molecular process or state of a disease. To this end, the most promising techniques are biophotonic technologies based on low-energy (optical) photons due to their low invasivity [1]. While biophotonic-based chemical imaging and sensing is not yet widely applied in real-world applications, many different technologies have been developed over the last few years that will be used in the near future.

The basic requirement for chemical imaging using biophotonic technologies is the optical detection of a chemical species or a chemical change. This requirement can be achieved by detecting the optical response of either an endogenous biomarker or a sensor sensitive to a specific chemical change. These processes are commonly referred to as optical biopsies, in contrast to the traditional physical biopsies,

which, in combination with histopathological exams, are the golden standard for the investigation of tissues. Optical biopsies offer advantages because they are minimally invasive and can give diagnostic information in real-time, as they do not require the excision of tissue samples and further *ex vivo* analysis. Furthermore, traditional biopsies are prone to false negative results due to sampling errors. Optical biopsies using various techniques including reflectance, fluorescence, and Raman scattering can give a complete examination of the organ of interest avoiding the sampling step. In this paper, we will discuss optical biopsies techniques including laser-induced fluorescence (LIF), Raman spectroscopy, and surface-enhanced Raman scattering (SERS), which have been developed in our laboratory for investigating specific biochemical markers.

Fluorescence was one of the first phenomenon studied in biophotonic technology for chemical imaging, due to its large photon output [2–4]. LIF-based chemical imaging can be performed by detecting exogenous and endogenous fluorophores. In the first case, fluorescent dyes introduced in the tissue are used for imaging; they take advantage of their ability to localize in tumors or their emission sensitivity to the local environment (e.g., pH or ions concentration). These types of techniques have the advantage of producing very strong signals; however, fluorescent dyes tend to photobleach and are usually toxic. Alternatively, endogenous fluorophores have also been used for tissue imaging and diagnostics. The fluorescence emission profile of tissues relays information that is closely tied to the concentrations of different fluorescent molecules. The use of a laser to stimulate the fluorescence in LIF has the advantage of increasing the fluorescence signal output and limiting the excitation to a specific wavelength, simplifying the emission profile and its origin determination. This technique has been used in cancer diagnostics for differentiation of malignant and healthy brain tissues via their distinct emission that is associated with their different metabolic states [5], as well as for applications ranging from cervical to arteriosus tissue monitoring [6–8]. However, fluorescence emission tends to have a very broad spectral profile given by the electronic transition associated with this emission, resulting in overlapping spectra that complicate the process of quantifying a specific chemical species.

The narrow spectral features associated with Raman spectroscopy confer several key advantages over fluorescence-based techniques for tissue diagnostics. This characteristic of Raman spectroscopy enables the simultaneous identification of multiple vibrational bands, which correspond to specific molecular species in the tissue. Raman is also not affected by photobleaching, and its excitation wavelength can be tuned, modifying the number of scattered photons without changing the spectrum characteristics. In spite of its many advantages, Raman scattering is an inherently low phenomenon, with only 1 out of  $10^{30}$  photons being scattered inelastically. This limitation hinders the translation of this technique into clinical technologies due to the complicated and costly instrumentation needed for the detection of the very few Raman photons. Recently, stimulated Raman imaging was used for the differentiation between malignant and healthy tissues *ex vivo*, further demonstrating how amplifying the Raman signal can enable the use of this information-rich spectroscopic technique for tissue diagnostics [9].

To overcome the limitations of conventional Raman spectroscopy, surface-enhanced Raman spectroscopy (SERS) can be used to enhance the Raman signal over a million fold ( $10^7$ – $10^{10}$  typically) by taking advantage of the unique interaction between light and metallic nanostructures and enabling the use of this phenomenon for analytical purposes [10–12]. Metals at the nanoscale can couple with photons at a certain frequency, producing a phenomenon called localized surface plasmon (LSP) [13,14], which consists of a collective excitation of the conduction band electrons on the surface of the metal. LSP enhances all the scattering phenomena in proximity and on the metallic surface, amplifying the Raman signal of molecules adsorbed or brought in contact to the surface of the metal. This plasmonic enhancement has led to the development of SERS and permitted the use of Raman for trace analysis in analytical applications while also promoting the integration of Raman with nanotechnologies [15,16]. Theoretical studies and numerical simulations have shown intense electromagnetic field enhancement in a wide variety of plasmonic structures [17–23]. While intrinsic SERS (i.e., the direct SERS detection of a target molecule) is useful for applications ranging from explosive traces detection and remote

aqueous analysis to cellular secretion identification [24–26], *in vivo* studies are limited to the use of extrinsic SERS, which consist of detecting a target indirectly via a SERS-based sensing mechanism. SERS-based technologies for chemical sensing and imaging consist of SERS nanoprobe and SERS sensors. The first are metallic nanoparticles coated with a Raman active molecule that accumulate in a specific type of cells/tissue (e.g., malignant tissues). Recently, SERS tags have been used for the detection of various type of cancer in intraoperative applications and have been shown to be able to detect cardio-vascular disease in a mouse model [27,28]. The second type of SERS nanoparticles (i.e., SERS-sensors) are coated with a molecular sensing system that will induce a change in the outputted Raman signal in the presence of a target. Extrinsic SERS-based chemical detection conserves all the advantages offered by Raman spectroscopy while amplifying the Raman signal of multiple orders of magnitude.

Our laboratory has introduced various biophotonics-based technologies for chemical sensing and imaging for diagnostic and research purposes. Over the years, we have developed a wide variety of fluorescence and SERS-based technologies for the detection of cancer and other diseases biomarkers. There have been previous reviews on chemical and biological sensors developed in various research groups [29–33]. This paper highlights the research activities in our laboratory for the development *in vivo* imaging and sensing, which includes the detection and localization of changes in the concentration of endogenous fluorophores associated with malignant tissue, the SERS-tag localization of cancer cells and tissues, and the SERS-based detection of nucleic acids and its feasibility for *in vivo* applications. We also discuss how the developed techniques worked on range of systems (from plants to animals and humans). Furthermore, this manuscript presents new development on the use of Raman imaging of SERS-labeled nanoprobe incubated in leaves for use in biofuel research.

## 2. Fluorescence-Based Technologies

### 2.1. Differential Normalized Light Induced Fluorescence

Endogenous fluorophores provide specific targets for molecular sensing *in vivo*. Several fluorophores such as reduced nicotinamide adenine dinucleotide (NADH) and flavin adenine dinucleotide (FAD) are involved in the cellular metabolism of cells, making them attractive targets for tissue disease classification [34]. Laser excitation in the ultraviolet range (350–400 nm) can specifically target these metabolic markers, and the resulting emission spectra can be correlated with the presence of diseases such as cancer. Other molecules such as collagen and elastin are also excited in this region and can also serve as a qualitative indicator of an abnormal extracellular environment if the fluorescence spectral features change significantly [34].

A significant limitation for this technique, however, is that the fluorescence emission is highly susceptible to many factors, ranging from uneven illumination of the target spot to inhomogeneous tissue composition at the target spot, resulting in an emission spectrum that can be very different between measurements. The first problem is particularly prevalent in situations in which instrument control is limited, such as during endoscopy procedures. Our group investigated this problem and came up with a technique known as Differential Normalized Fluorescence (DNF) [4]. This method involves normalizing all the fluorescence measurements to a baseline reference spectrum from normal tissue. In doing so, small spectral shape differences are magnified and can be attributed to the addition or depletion of certain molecules in target areas.

This technique was first applied to the detection and diagnosis of gastrointestinal (GI) cancer and Barrett's esophagus, a premalignant condition of esophageal cancer [4]. The device shown in Figure 1A is an endoscope that is coupled to a 410-nm laser and a photodetector interfaced with a computer. The device can be used as a clinical tool to probe the esophageal lining without the need for biopsy. Figure 1B shows that the DNF transformed spectrum can be delineated from the DNF of normal tissue. The large trough in the malignant tissue DNF at 480 nm in particular can be used to quickly classify different tissue regions, providing an indication of a positive or negative diagnosis of Barrett's

esophagus. Over 400 measurements on more than 100 patients were used in this study; the study resulted in only 1 misclassification out of 114 samples and even revealed malignancy in tissues missed by biopsy. Further studies with this system looked for the presence of reactive atypia/inflammation to differentiate from non-dysplastic Barrett's esophagus with low-grade dysplasia and produced similarly excellent results with 96% of non-dysplastic Barrett's and low-grade dysplasia correctly classified as benign and over 90% of high-grade dysplasia correctly classified as premalignant [35].

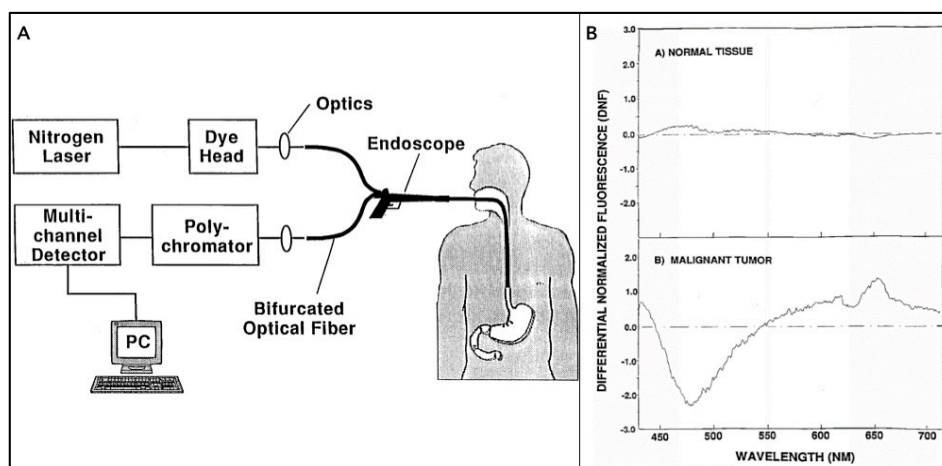


**Figure 1.** (A) Schematic diagram of the instrumental system used for laser-induced fluorescence diagnosis of esophageal cancer. (B) Example of a differential normalized fluorescence curve of (A) a normal esophageal mucosa; (B) an esophageal adenocarcinoma. The DNF curve (B) clearly shows the negative peak at  $475 \pm 480$  nm, which is characteristic of malignant tissue in the esophagus. Adapted from [4].

## 2.2. Hyperspectral Fluorescence Imaging

While the above method of detecting malignant tissue provided a useful alternative to traditional biopsies, the modality is limited to only analyzing a spectrum of selected points. Our group improved on the device by incorporating another light source (white light) to produce a reflectance image and an acousto-optic tunable filter (AOTF) to scan the different wavelengths of the fluorescence emission [36]. With these additions, fluorescence images at different wavelengths can be taken simultaneously with a normal image, allowing for the co-registration of the spatial locations of fluorescent molecules with the physical features of the tissue. This modality, known as hyperspectral fluorescence imaging (HFI), produces a hyper-cube dataset that contains a stack of fluorescence images that represents different wavelengths. This capability gives this system a unique advantage in producing images whose pixels represent a single data point of a spectrum, allowing very high throughput and giving a wealth of data for processing. By scanning the emission wavelengths with the AOTF, one can focus in on the expected emission maximum of specific fluorophores and estimate their amount in different regions of the image. For example, having the AOTF set to 450 nm would give as an image representative of the fluorescence of FAD, NADH, and collagen while having it set at 630 nm would give as an image of porphyrin molecules. Another distinct advantage of this system is its capability to delineate which parts of the tissue are fluorescent relative to other regions, solving the tissue inhomogeneity problem of the previous system.

Figure 2 shows the overall setup with the resulting fluorescence and reflectance image side by side. Studies performed on mouse skin tumor models showed great spatial registration with reflectance images. As before, the ability to identify malignant tissue intraoperatively is a significant advantage over biopsies and can help guide decisions during surgery. While there are clear differences between pixels in an image, additional processing techniques can improve the effectiveness of classification. Techniques such as support vector machines (SVM) are used on the hyperspectral data cube, training

the model to classify tumor and non-tumor data [37]. A receiver operating curve (ROC) plots the true positive rate against the false positive rate, with a number between 0 and 1, in which 0.5 is not a very good and 1 is perfect. The model created with 100 samples with 21 spectral bands (divisions of spectral regions) each produced a very good discrimination value of 0.9613. The number of spectral bands to split into can also be reduced to improve imaging throughput and speed, and as few as two bands can be used to retain a reasonably high ROC of 0.9829. Hyperspectral Fluorescence Imaging can give all the fluorescence information about a sample, but it is also very flexible and can be changed to acquire only specific spectral bands when speed is more important.

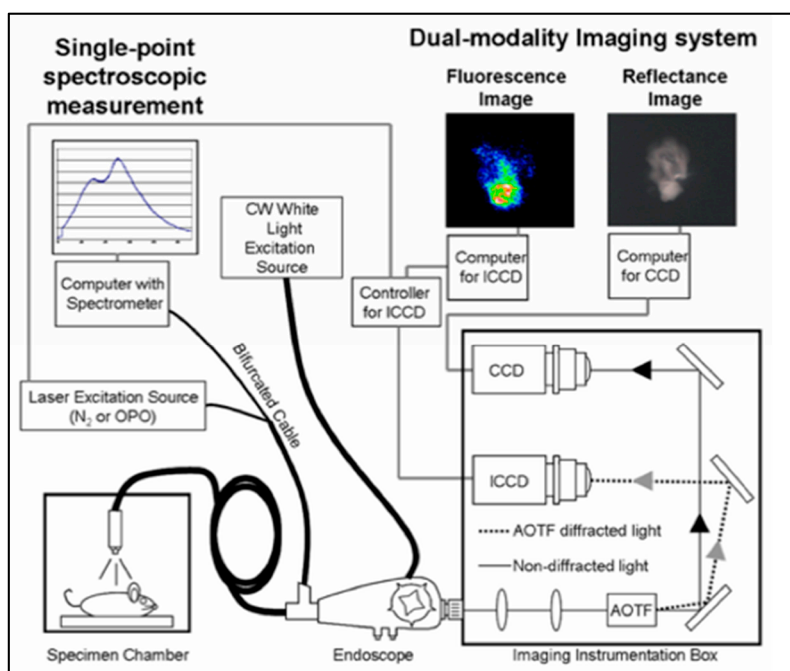


**Figure 2.** Hardware components of the hyperspectral imaging system with expletive fluorescence hyperspectral and reflectance images of a tumor. Adapted from [37].

### 3. SERS-Based Technologies

#### 3.1. SERS Nanoprobes

As described in the introduction, the use of SERS nanoprobes in diagnostic tools provides a marked improvement over fluorescence-based methods by increasing the number of simultaneous biomarker detections. Initial work on SERS nanoprobes imaging was performed with silver colloids *in vitro*. Silver colloids were used to take advantage of the strong enhancement that can be achieved in the gaps between nanoparticles (nano-gaps) [38]. The colloids were fabricated by silver nanoparticles synthesis and sequential salt-dependent aggregation, before coating them with a dye—crystal violet. Cells were then incubated with the colloids for several days, washed, and fixed to be imaged. The imaging setup consisted of an inverted microscope coupled with a HeNe laser for Kohler epi-illumination and a tungsten lamp used for transmission illumination. The image from the microscope is passed through a holographic notch filter and an AOTF, which generates a 0th order image and a narrowly filtered 1st order image. The two images are collected in two different cameras. Figure 3 shows a comparison between a bright field image (A) and the image from the total SERS signal (B) of a fixed cell; the two images are merged in (C). The results demonstrated that the system was able to localize the SERS nanoprobes inside single cells and to obtain Raman spectra from intracellular cell nanoprobes [39]. As seen in Figure 3, the SERS signal localized in the cell is inhomogeneous in contrast with the particles distribution observed via fluorescence, which was

found to be homogenous throughout the cell [39]. This issue was attributed to the difference in SERS enhancement across the colloids produced by random aggregation. Though these results do not show structural characterization of biomolecular components within a cell, these experiments proved that the hyperspectral system has the capability to localize un-targeted labeled nanoparticles within a cell using SERS.

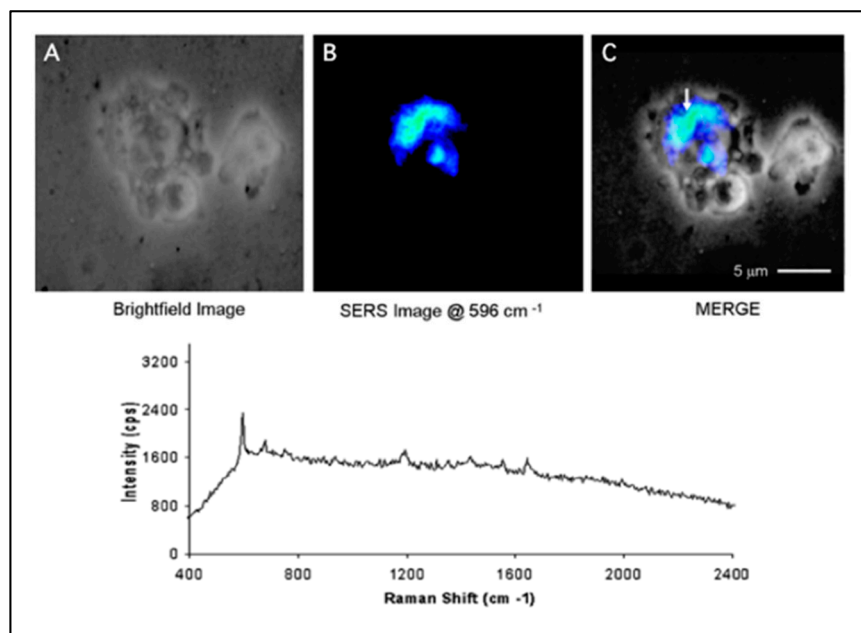


**Figure 3.** SERS images and spectra of CHO cells incubated with cresyl violet-labeled silver colloidal particles. The bright field image (A), the total SERS image (B), and the merged image (C) of a fixed cell are shown. The arrow indicates regions within the cell where clusters of silver nanostructures are located. The SERS image was acquired at a SERS intensity signal of  $596\text{ cm}^{-1}$  using a  $632.8\text{ nm}$  HeNe laser for excitation. Scale bars are of  $5\text{ }\mu\text{m}$ . Adapted from [39].

While colloidal aggregates offer very large SERS enhancement due to the presence of nano-gaps, the randomness of the aggregation process makes them incapable of being used for quantification. Alternatively, single spherical metallic nanoparticles have much smaller enhancement factors, which limit their sensitivity in analytical applications. To improve the SERS enhancement of single nanoparticles, different shapes and materials have been used to fabricate nanostructures with increased enhancement factors [40–43]. Our lab has developed a class of branched nanoparticles called gold nanostars (GNS), which generate strong SERS enhancement factors due to the lightning rod effect (i.e., accumulation of surface charges) experienced at the tip of the branches [42,44]. The use of GNSs in place of silver colloids has several advantages, such as biocompatibility and homogeneity, while conserving a large SERS enhancement factor [44,45].

Further experiments on SERS nanoprobe *in vitro* explored the use of silica coated GNSs conjugated with active targeting molecules. The biocompatibility of these SERS nanoprobe is due to the silica coating, which creates a barrier between the toxic silver surface and the cell. The particles were rendered SERS-active by coating the surface of the GNSs with mercaptobenzoic acid (MBA). The active targeting was obtained by functionalizing the silica shell of these SERS nanoprobe with folic acid that is recognized by the folate receptor (FR), overexpressed in many cancer cells. An *in vitro* demonstration of the SERS-based diagnostics was performed by incubating the particles with two FR-positive cell lines (HeLa and SK-BR-3) and one FR-negative cell line (MDA-MB-468). Figure 4 shows an overlap of bright field images and Raman maps obtained for the different cell lines [46]. In contrast with Figure 3, these results were obtained on a raster-scanning system with a reduction

in the resolution of the Raman image. As shown in Figure 4, both the FR-positive cell lines show high signal intensity from the folate-targeted nanoparticles, with a low background signal outside of the cell-containing region [46]. The selective detection of FR-positive cells was demonstrated using Raman imaging, showing a high SERS signal from the FR-positive cells and little to no signal from the FR-negative cells.

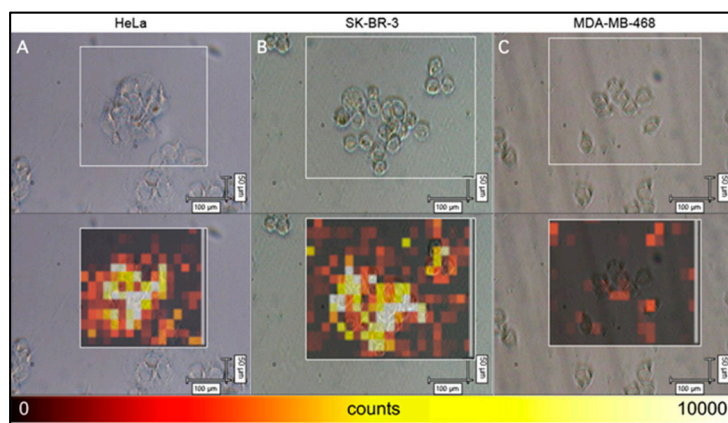


**Figure 4.** Raman mapping of the three different cell lines after 4 h incubation with the FA-targeted theranostic nanoparticles at 0.1 nM concentration. The sample was scanned in a grid pattern with 20  $\mu\text{m}$  step size, taking a 1 s acquisition at each point. The Raman peak intensity at each point was then integrated to create the false-color Raman map that is overlaid on the bright field image. Raman maps correspond to 2 FR-positive cell lines, HeLa (A), and SK-BR-2 (B), and a FR-negative cell line, MDA-MB-468 (C). The FR-positive cell lines show high Raman intensity coming from the cluster of cells, whereas the FR-negative cell line shows little to no Raman signal. Scale bars are X = 100  $\mu\text{m}$  and Y = 50  $\mu\text{m}$ . Adapted from [46].

To prove the possibility of using SERS nanoprobe as a clinical tool, studies were done using SERS-active particles on animal models such as rats and pigs. Gold nanostars coated with dyes were incorporated into biocompatible polymer scaffold and inserted under the skin animal. The GNSs used as nanoprobe in this experiment were both silica coated and bare GNSs. The polymer used for the SES nanoprobe implantation was a porous poly(2-hydroxyethylmethacrylate) hydrogel developed for this purpose [47]. In both the animal models, the SERS signal from the nanoprobe was identified. The experiments *in vivo* were performed with NIR laser excitation (785 nm) to limit the tissue autofluorescence. The results from these *in vivo* tests demonstrated that the GNSs could be detected *in vivo* in animal tissue. Furthermore, the results shown in Figure 5 demonstrate that SERS signals can still be detected 6 days following implantation, thus underlining the possibility for long-term sensing applications [48]. Although the SERS signal was greatly attenuated through tissue, the optimal combinations of several strategies, including use of efficient plasmonic structure like the GNS, excitation, and detection inside the tissue optical window, and intradermal implantation of GNSs in the sub-dermal tissue layer, are a straightforward and efficient strategy of maximizing SERS signal for *in vivo* monitoring. It was also shown that gold nanostars can be incorporated into tissue-integrating polymer scaffolds, implanted in live animals, and monitored over long periods of time.

As a further step towards their clinical use, SERS nanoprobe were used to localize a tumor in a mouse *in vivo*. Gold nanostars tagged with the MBA Raman reporter were coated with polyethylene glycol (PEG), to prolong their circulation time *in vivo*, and injected in the tail vein of a mouse with a primary soft tissue sarcoma grown on the flank. The GNSs accumulated into and around the tumor tissue due to a process known as enhanced permeability and retention (EPR), which permits particles of a size ranging between 10–100 nm to be uptaken by the leaky tumor vasculature [49]. One day

after the injection, SERS spectra were obtained from healthy and from cancer muscular tissue of the anesthetized mouse, using NIR laser excitation and a fiber-optic probe. Figure 6 shows the SERS spectra and the location from which they were obtained, and these signals were notably only seen around the tumor areas [50]. These results demonstrated how SERS nanoprobes can potentially be used for cancer localization *in vivo* and for SERS-based tumor imaging.

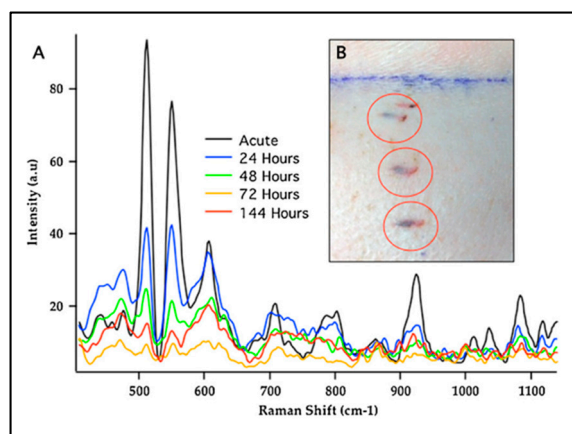


**Figure 5.** (A) SERS Spectra of Cy7-labeled NS embedded in porous scaffold and intradermally implanted in pig dorsum (100 ms acquisitions, 30 mW, 785 nm excitation). (B) Three individual intradermally injected implants after 48 h. Adapted from [48].

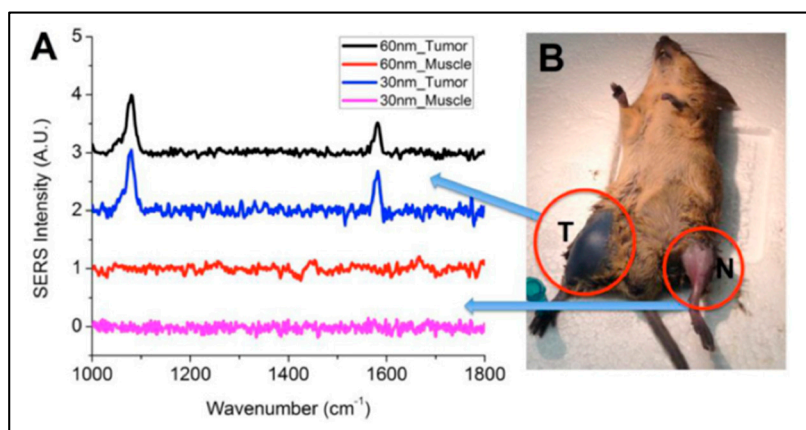


**Figure 6.** (A) *In vivo* SERS spectra of 30-nm and 60-nm GNS nanoprobes with MBA reporter. Unique SERS peaks can be detected at 1067 and 1588  $\text{cm}^{-1}$  in the tumor, but not in the normal muscle. The spectra are offset for visualization. (B) Mouse with primary sarcomas 3 days after 30-nm GNS injection. Significant GNS accumulation can be seen in the tumor (T) but not in the normal leg muscle of the contralateral leg (N). Adapted from [50].

### 3.2. SERS Sensors

SERS sensors have a different role with respect to SERS nanoprobes owing to their ability to detect and quantify a specific target or biomarker. Our group has developed a class of SERS sensors called “molecular sentinels” (MS) that can detect nucleic acid biotargets (e.g., DNA, mRNA, and miRNA) [51–53]. The MS sensing is composed of a nucleic acid probe strand bound to a SERS active surface and terminated with a Raman reporter molecule. The SERS signal from the Raman reporter is highest when in contact with or in close proximity to the metallic surface of the nanoparticle. The MS sequence is designed to naturally form a stem-loop, which controls the distance between the reporter and the surface of the nanoparticle. In the absence of target strand, the stem loop configuration

of the MS will have the Raman reporter close to the nanoparticle and thus give an “on” SERS signal. Once the target sequence is introduced, it will partially bind to the complementary sequence on the MS and subsequently straighten out the stem loop. This brings the Raman reporter farther away from the plasmonics-active surface which turns “off” the SERS signal. Inverse molecular sentinels (iMS) were developed to improve over the initial design by changing the mechanism to an ‘off-to-on signal’ instead, which increases the limit of detection by reducing the shot noise [54]. The iMS works by binding a placeholder (i.e., a DNA strand complementary to the target sequence) to the molecular sentinel strand to lock the probe in an open position. The stem-loop is thus only permitted to close in the presence of the target sequence through strand displacement of the placeholder-probe complex. The diagnostic capabilities of these sensors have been demonstrated by detecting different expression of miRNA in different cancer cell lines [54]. The MS and iMS detection schemes have been further adapted and integrated to a chip platform for medical diagnostics [55–57]. A “smart tattoo” biosensor using iMS nanoprobe has been developed for the detection of synthetic nucleic acid targets in a large animal model *in vivo* [58].

Recently, our group has been integrating the iMS sensing modality with an imaging system to achieve SERS-based functional imaging. Such a system would be able to study the molecular pathways associated with specific nucleic acid targets *in vivo* with the temporal and spatial resolution required to understand the mechanisms behind the regulatory role of nucleic acids. This knowledge is particularly important in plant biology, in which miRNAs are known to be a factor in the stimulus-dependent regulation between phases of a plant life-cycle, which has implications for biofuel production [59]. A more complete comprehension of the role of miRNA would allow for the engineering of plants as better bioenergy sources. SERS nanoprobe technologies could provide the much needed tool to detect miRNA biomarkers *in vivo* without target extraction and amplification.

To prove the feasibility of *in vivo* SERS chemical imaging in plants, we delivered a solution of GNSs coated with a dye used in the iMS (Cy7), a tobacco leaf that uses needleless injection. The solution contained GNSs at a 1 nM concentration in a PBS buffer containing 0.01% Tween-20. The GNSs used in this experiment were coated with a thiolated and dye-conjugated short (MW = 1000) PEG chain (HS-PEG(1k)-Cy7 from Nanocs) and a longer (MW = 5000) thiolated PEG chain (HS-PEG(5k) from Nanocs) to improve the particles stability in buffer. Approximately 20  $\mu\text{L}$  of the solution was infiltrated and spread in a total area of 1  $\text{cm}^2$ . Raman maps of the infiltrated leaf were measured with a lab-built Raman microscope composed of an inverted microscope coupled to a 300 mW 785 nm diode laser (from Optoengine) focused on the image plane of the microscope objective (laser spot = 500  $\mu\text{m}$ ). The objective used in the experiment was selected to maximize the field of view and detect whole-leaf images (2X NA = 0.1 from Thorlabs). The mapping images were obtained using a lab-developed Labview code, which automated the stage movements (100 mm  $\times$  120 mm travel RS-232 from Zaber) and coordinated the spectra acquisition (LS785 and Pixis100 from Princeton Instruments). The movements were of 600  $\mu\text{m}$  and the spectra integrated for 10 times for 0.1 s per point. A bright field image was taken before each map with a CCD camera (ProEM 512B from Princeton Instruments) connected to the microscope, to correlate the Raman and transmission images. The background subtraction and smoothing of the spectra was performed on Matlab using a Savitsky-Golay filter (five-point window and first-order polynomial).

Figure 7 shows the results from the infiltration of the tobacco leaf. The leaf was infiltrated in a spot on the bottom left of the image (Figure 7B), and the particles spread radially but homogeneously from the spot. The infiltrated area is visible in Figure 7B as the lighter (more transmission) area, which is due to the liquid spreading inside the leaf. Raman map of the 1119  $\text{rel. cm}^{-1}$  background subtracted peak was superimposed over the original microscope image of the leaf and is shown in Figure 7A. The particles signal is also spread radially from the injection point, as expected. Figure 7C shows the background subtracted spectra from a single pixel from an image of an infiltrated leaf and of the leaf prior to the infiltration. While the spectrum before the infiltration shows some peaks coming from the optics and the leaf, the spectrum from the infiltrated leaf exhibits a much stronger Raman signal and

the characteristic peaks of Cy7. These results demonstrate the possibility to obtain a SERS map of the leaf, which reflects the locations of GNSs infiltrated in the leaf. This SERS imaging capability will lay the foundation for studies on functional imaging of nucleic acids in plants.

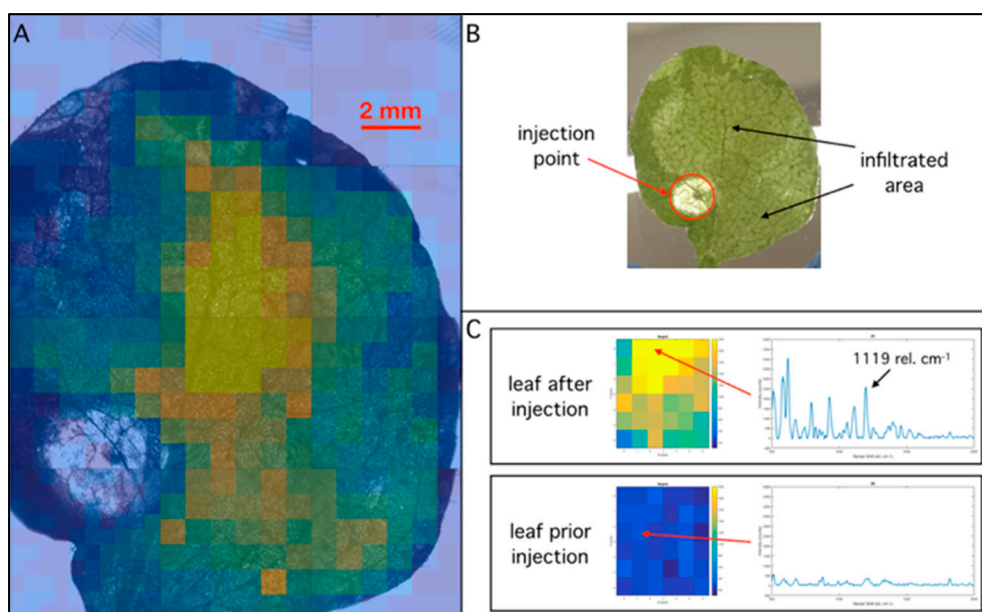


**Figure 7.** (A) Background subtracted Raman map ( $1119 \text{ rel. cm}^{-1}$ ) superimposed to its respective bright field image of a leaf infiltrated with labeled nanostars. (B) Image of the infiltrated leaf. (C) Raman maps of a section of the leaf before and after the injection of the nanostars. The spectra from one of the pixel of each map (indicated by the arrow) are shown on the side of the maps.

#### 4. Conclusions and Perspective

In summary, our laboratory has developed a wide variety of novel biophotonic technologies for chemical sensing and imaging. Laser-induced fluorescence was developed to detect endogenous fluorophores in order to identify malignant cancerous tissues. The fluorescence technique was further expanded into a hyperspectral imaging modality capable of imaging the malignant tissue. SERS nanoprobe were developed for sensing *in vitro* inside single cells and used to target overexpressed receptors in cancerous cell lines. This type of probe was also detected in animal tissue and demonstrated to be stable over several days. EPR accumulation of SERS-labeled GNSs in tumors was used to detect malignant tissue in a live animal model using SERS detection. Furthermore, SERS probes were also detected in infiltrated leaves, illustrating the capabilities of SERS-based technologies for plant studies in biofuel research.

Biophotonic technologies have received increasing interest in clinical settings for *in vivo* applications; examples are the use of laser-ablation therapy and fluorescence-guided surgery. While fluorescence-based applications have already been widely used in clinical settings contributing to the advancement of clinical diagnostics, SERS has yet to be introduced for wider *in vivo* clinical use. Currently, much research is being devoted to better understanding the potential health effects and properties of SERS-active nanomaterials for *in vivo* use. In this respect, gold has been demonstrated to be a biocompatible, non-toxic SERS-active material. Although SERS has not yet been adopted *in vivo*, many *ex vivo* applications have shown the potential of this technique for the detection of biotargets. The main advantages of replacing fluorescence with SERS for the detection of biotargets are the multiplexability of Raman reporters and their diagnostic accuracy. Once nanotechnology is accepted for clinical applications, SERS-based biophotonic technologies will permit the achievement of previously unmet goals, such as the functional imaging of biotargets, for research purposes,

and highly multiplexed sensors for the simultaneous and direct detection of large panels of biotargets, for diagnostic purposes.

**Acknowledgments:** This material is based upon work supported by the National Institutes of Health (1R21CA196426), by the U.S. Department of Energy Office of Science, under Award Number DE-SC0014077, and by the Duke Faculty Exploratory Research Fund.

**Conflicts of Interest:** The authors declare no conflict of interest.

## References

1. Vo-Dinh, T. *Biomedical Photonics Handbook: Biomedical Diagnostics*, 2nd ed.; CRC Press: Boca Raton, FL, USA, 2014.
2. Lipson, R.L.; Baldes, E.J.; Olsen, A.M. The Use of a Derivative of Hematoporphyrin in Tumor Detection. *JNCI: J. Natl. Cancer Inst.* **1961**, *26*, 1–11. [[PubMed](#)]
3. Andersson-Engels, S.; af Klinteberg, C.; Svanberg, K.; Svanberg, S. In vivo fluorescence imaging for tissue diagnostics. *Phys. Med. Biol.* **1997**, *42*, 815. [[CrossRef](#)] [[PubMed](#)]
4. Vo-Dinh, T.; Panjehpour, M.; Overholt, B.F.; Buckley III, P. Laser-Induced Differential Fluorescence for Cancer Diagnosis without Biopsy. *Appl. Spectrosc.* **1997**, *51*, 58–63. [[CrossRef](#)]
5. Liu, Q.; Grant, G.; Li, J.; Zhang, Y.; Hu, F.; Li, S.; Wilson, C.; Chen, K.; Bigner, D.; Vo-Dinh, T. Compact point-detection fluorescence spectroscopy system for quantifying intrinsic fluorescence redox ratio in brain cancer diagnostics. *J. Biomed. Opt.* **2011**, *16*, 037004. [[CrossRef](#)] [[PubMed](#)]
6. Ramanujam, N.; Mitchell, M.F.; Mahadevan, A.; Warren, S.; Thomsen, S.; Silva, E.; Richards-Kortum, R. In vivo diagnosis of cervical intraepithelial neoplasia using 337-nm-excited laser-induced fluorescence. *Proc. Natl. Acad. Sci. USA* **1994**, *91*, 10193. [[PubMed](#)]
7. Schomacker, K.T.; Frisoli, J.K.; Compton, C.C.; Flotte, T.J.; Richter, J.M.; Deutsch, T.F.; Nishioka, N.S. Ultraviolet laser-induced fluorescence of colonic polyps. *Gastroenterology* **1992**, *102*, 1155–1160. [[CrossRef](#)]
8. Deckelbaum, L.I.; Lam, J.K.; Cabin, H.S.; Clubb, K.S.; Long, M.B. Discrimination of normal and atherosclerotic aorta by laser-induced fluorescence. *Lasers Surg. Med.* **1987**, *7*, 330–335. [[CrossRef](#)] [[PubMed](#)]
9. Orringer, D.A.; Pandian, B.; Niknafs, Y.S.; Hollon, T.C.; Boyle, J.; Lewis, S.; Garrard, M.; Hervey-Jumper, S.L.; Garton, H.J.L.; Maher, C.O.; et al. Rapid intraoperative histology of unprocessed surgical specimens via fibre-laser-based stimulated Raman scattering microscopy. *Nat. Biomed. Eng.* **2017**, *1*, 0027. [[CrossRef](#)] [[PubMed](#)]
10. Jeanmaire, D.L.; Van Duyne, R.P. Surface raman spectroelectrochemistry: Part I. Heterocyclic, aromatic, and aliphatic amines adsorbed on the anodized silver electrode. *J. Electroanal. Chem. Interfacial Electrochem.* **1977**, *84*, 1–20. [[CrossRef](#)]
11. Moskovits, M. Surface-enhanced spectroscopy. *Rev. Mod. Phys.* **1985**, *57*, 783. [[CrossRef](#)]
12. Vo-Dinh, T.; Hiromoto, M.Y.K.; Begun, G.M.; Moody, R.L. Surface-enhanced Raman spectrometry for trace organic analysis. *Anal. Chem.* **1984**, *56*, 1667–1670. [[CrossRef](#)]
13. Maier, S.A. *Plasmonics: Fundamentals and Applications*; Springer: New York, NY, USA, 2007.
14. Kelly, K.L.; Coronado, E.; Zhao, L.L.; Schatz, G.C. The Optical Properties of Metal Nanoparticles: The Influence of Size, Shape, and Dielectric Environment. *J. Phys. Chem. B* **2003**, *107*, 668–677. [[CrossRef](#)]
15. Strobbia, P.; Languirand, E.; Cullum, B.M. Recent advances in plasmonic nanostructures for sensing: A review. *Opt. Eng.* **2015**, *54*, 100902. [[CrossRef](#)]
16. Vo-Dinh, T. Surface-enhanced Raman spectroscopy using muctureetallic nanostrs. *TrAC Trends Anal. Chem.* **1998**, *17*, 557–582. [[CrossRef](#)]
17. Dhawan, A.; Norton, S.J.; Gerhold, M.D.; Vo-Dinh, T. Comparison of FDTD numerical computations and analytical multipole expansion method for plasmonics-active nanosphere dimers. *Opt. Express* **2009**, *17*, 9688–9703. [[CrossRef](#)] [[PubMed](#)]
18. Khoury, C.G.; Norton, S.J.; Vo-Dinh, T. Plasmonics of 3-D Nanoshell Dimers Using Multipole Expansion and Finite Element Method. *ACS Nano* **2009**, *3*, 2776–2788. [[CrossRef](#)] [[PubMed](#)]
19. Norton, S.J.; Vo-Dinh, T. Plasmon Resonances of Nanoshells of Spheroidal Shape. *IEEE Trans. Nanotechnol.* **2007**, *6*, 627–638. [[CrossRef](#)] [[PubMed](#)]
20. Norton, S.J.; Vo-Dinh, T. Optical response of linear chains of metal nanospheres and nanospheroids. *J. Opt. Soc. Am. A* **2008**, *25*, 2767–2775. [[CrossRef](#)]

21. Norton, S.J.; Vo-Dinh, T. Spectral bounds on plasmon resonances for Ag and Au prolate and oblate nanospheroids. *J. Nanophotonics* **2008**, *2*, 029501. [[CrossRef](#)] [[PubMed](#)]
22. Norton, S.J.; Vo-Dinh, T. Plasmonics enhancement of a luminescent or Raman-active layer in a multilayered metallic nanoshell. *Appl. Opt.* **2009**, *48*, 5040–5049. [[CrossRef](#)] [[PubMed](#)]
23. Vo-Dinh, T.; Dhawan, A.; Norton, S.J.; Khoury, C.G.; Wang, H.-N.; Misra, V.; Gerhold, M.D. Plasmonic Nanoparticles and Nanowires: Design, Fabrication and Application in Sensing. *J. Phys. Chem. C* **2010**, *114*, 7480–7488. [[CrossRef](#)] [[PubMed](#)]
24. Farrell, M.E.; Holthoff, E.L.; Pellegrino, P.M. Surface-Enhanced Raman Scattering Detection of Ammonium Nitrate Samples Fabricated Using Drop-on-Demand Inkjet Technology. *Appl. Spectrosc.* **2014**, *68*, 287–296. [[CrossRef](#)] [[PubMed](#)]
25. Bello, J.M.; Narayanan, V.A.; Stokes, D.L.; Vo-Dinh, T. Fiber-optic remote sensor for in situ surface-enhanced Raman scattering analysis. *Anal. Chem.* **1990**, *62*, 2437–2441. [[CrossRef](#)]
26. Lussier, F.; Brulé, T.; Vishwakarma, M.; Das, T.; Spatz, J.P.; Masson, J.-F. Dynamic-SERS Optophysiology: A Nanosensor for Monitoring Cell Secretion Events. *Nano Lett.* **2016**, *16*, 3866–3871. [[CrossRef](#)] [[PubMed](#)]
27. Karabeber, H.; Huang, R.; Iacono, P.; Samii, J.M.; Pitter, K.; Holland, E.C.; Kircher, M.F. Guiding Brain Tumor Resection Using Surface-Enhanced Raman Scattering Nanoparticles and a Hand-Held Raman Scanner. *ACS Nano* **2014**, *8*, 9755–9766. [[CrossRef](#)] [[PubMed](#)]
28. Noonan, J.; Grassia, G.; Macritchie, N.; Asiala, S.; Gracie, K.; Faulds, K.; McInnes, I.B.; Garside, P.; Graham, D.; Maffia, P. Multiplex detection of endothelial cell activation biomarkers using surface enhanced raman spectroscopy (sers). *Atherosclerosis* **2017**, *263*, e1–e18. [[CrossRef](#)]
29. Probst, R.; Gahlen, J. Fluorescence diagnosis of colorectal neoplasms: A review of clinical applications. *Int. J. Colorectal Dis.* **2002**, *17*, 1–10. [[CrossRef](#)] [[PubMed](#)]
30. DSouza, A.V.; Lin, H.; Henderson, E.R.; Samkoe, K.S.; Pogue, B.W. Review of fluorescence guided surgery systems: Identification of key performance capabilities beyond indocyanine green imaging. *J. Biomed. Opt.* **2016**, *21*, 080901. [[CrossRef](#)] [[PubMed](#)]
31. Yun, S.H.; Kwok, S.J.J. Light in diagnosis, therapy and surgery. *Nat. Biomed. Eng.* **2017**, *1*, 0008. [[CrossRef](#)] [[PubMed](#)]
32. Henry, A.-I.; Sharma, B.; Cardinal, M.F.; Kurouski, D.; Van Duyne, R.P. Surface-Enhanced Raman Spectroscopy Biosensing: In Vivo Diagnostics and Multimodal Imaging. *Anal. Chem.* **2016**, *88*, 6638–6647. [[CrossRef](#)] [[PubMed](#)]
33. Laing, S.; Jamieson, L.E.; Faulds, K.; Graham, D. Surface-enhanced Raman spectroscopy for in vivo biosensing. *Nat. Rev. Chem.* **2017**, *1*, 0060. [[CrossRef](#)]
34. Wagnieres, G.A.; Star, W.M.; Wilson, B.C. In Vivo Fluorescence Spectroscopy and Imaging for Oncological Applications. *Photochem. Photobiol.* **1998**, *68*, 603–632. [[CrossRef](#)] [[PubMed](#)]
35. Panjehpour, M.; Overholt, B.F.; Vo-Dinh, T.; Coppola, D. The effect of reactive atypia/inflammation on the laser-induced fluorescence diagnosis of non-dysplastic Barrett's esophagus. *Lasers Surg. Med.* **2012**, *44*, 390–396. [[CrossRef](#)] [[PubMed](#)]
36. Vo-Dinh, T. A hyperspectral imaging system for in vivo optical diagnostics. *IEEE Eng. Med. Biol. Mag.* **2004**, *23*, 40–49. [[PubMed](#)]
37. Kong, S.G.; Martin, M.; Vo-Dinh, T. Hyperspectral Fluorescence Imaging for Mouse Skin Tumor Detection. *Etri J.* **2006**, *28*, 770–776. [[CrossRef](#)]
38. Moskovits, M. Surface-enhanced Raman spectroscopy: A brief retrospective. *J. Raman Spectrosc.* **2005**, *36*, 485–496. [[CrossRef](#)]
39. Wabuye, M.B.; Yan, F.; Griffin, G.D.; Vo-Dinh, T. Hyperspectral surface-enhanced Raman imaging of labeled silver nanoparticles in single cells. *Rev. Sci. Instrum.* **2005**, *76*, 063710. [[CrossRef](#)]
40. Jackson, J.B.; Halas, N.J. Surface-enhanced Raman scattering on tunable plasmonic nanoparticle substrates. *Proc. Natl. Acad. Sci. USA* **2004**, *101*, 17930. [[CrossRef](#)] [[PubMed](#)]
41. Orendorff, C.J.; Gearheart, L.; Jana, N.R.; Murphy, C.J. Aspect ratio dependence on surface enhanced Raman scattering using silver and gold nanorod substrates. *Phys. Chem. Chem. Phys.* **2006**, *8*, 165–170. [[CrossRef](#)] [[PubMed](#)]
42. Khoury, C.G.; Vo-Dinh, T. Gold Nanostars For Surface-Enhanced Raman Scattering: Synthesis, Characterization and Optimization. *J. Phys. Chem. C* **2008**, *112*, 18849–18859. [[CrossRef](#)]

43. Li, H.; Cullum, B.M. Dual Layer and Multilayer Enhancements from Silver Film over Nanostructured Surface-Enhanced Raman Substrates. *Appl. Spectrosc.* **2005**, *59*, 410–417. [[CrossRef](#)] [[PubMed](#)]
44. Yuan, H.; Fales, A.M.; Khoury, C.G.; Liu, J.; Vo-Dinh, T. Spectral characterization and intracellular detection of Surface-Enhanced Raman Scattering (SERS)-encoded plasmonic gold nanostars. *J. Raman Spectrosc.* **2013**, *44*, 234–239. [[CrossRef](#)] [[PubMed](#)]
45. Fales, A.M.; Yuan, H.; Vo-Dinh, T. Development of Hybrid Silver-Coated Gold Nanostars for Nonaggregated Surface-Enhanced Raman Scattering. *J. Phys. Chem. C* **2014**, *118*, 3708–3715. [[CrossRef](#)] [[PubMed](#)]
46. Fales, A.M.; Crawford, B.M.; Vo-Dinh, T. Folate Receptor-Targeted Theranostic Nanoconstruct for Surface-Enhanced Raman Scattering Imaging and Photodynamic Therapy. *ACS Omega* **2016**, *1*, 730–735.
47. Cho, E.H.; Boico, A.; Wisniewski, N.A.; Gant, R.; Helton, K.L.; Brown, N.L.; Register, J.K.; Vo-Dinh, T.; Schroeder, T.; Klitzman, B. Micovascular integration into porous polyHEMA scaffold. In Proceedings of the SPIE, Bioinspired, Biointegrated, Bioengineered Photonic Devices II, San Francisco, CA, USA, 3 March 2014; Volume 8958, p. 4.
48. Register, J.K.; Fales, A.M.; Wang, H.-N.; Norton, S.J.; Cho, E.H.; Boico, A.; Pradhan, S.; Kim, J.; Schroeder, T.; Wisniewski, N.A.; Klitzman, B.; Vo-Dinh, T. In vivo detection of SERS-encoded plasmonic nanostars in human skin grafts and live animal models. *Anal. Bioanal. Chem.* **2015**, *407*, 8215–8224. [[CrossRef](#)] [[PubMed](#)]
49. Greish, K. Enhanced Permeability and Retention (EPR) Effect for Anticancer Nanomedicine Drug Targeting. In *Cancer Nanotechnology: Methods and Protocols*; Grobmyer, R.S., Moudgil, M.B., Eds.; Humana Press: Totowa, NJ, USA, 2010; p. 25.
50. Liu, Y.; Ashton, J.R.; Moding, E.J.; Yuan, H.; Register, J.K.; Fales, A.M.; Choi, J.; Whitley, M.J.; Zhao, X.; Qi, Y.; et al. A Plasmonic Gold Nanostar Theranostic Probe for In Vivo Tumor Imaging and Photothermal Therapy. *Theranostics* **2015**, *5*, 946–960. [[CrossRef](#)] [[PubMed](#)]
51. Vo-Dinh, T.; Houck, K.; Stokes, D.L. Surface-Enhanced Raman Gene Probes. *Anal. Chem.* **1994**, *66*, 3379–3383. [[CrossRef](#)] [[PubMed](#)]
52. Wang, H.-N.; Vo-Dinh, T. Multiplex detection of breast cancer biomarkers using plasmonic molecular sentinel nanoprobe. *Nanotechnology* **2009**, *20*, 065101. [[CrossRef](#)] [[PubMed](#)]
53. Wang, H.-N.; Fales, A.M.; Vo-Dinh, T. Plasmonics-based SERS nanobiosensor for homogeneous nucleic acid detection. *Nanomedicine* **2015**, *11*, 811–814. [[CrossRef](#)] [[PubMed](#)]
54. Wang, H.-N.; Crawford, B.M.; Fales, A.M.; Bowie, M.L.; Seewaldt, V.L.; Vo-Dinh, T. Multiplexed Detection of MicroRNA Biomarkers Using SERS-Based Inverse Molecular Sentinel (iMS) Nanoprobes. *J. Phys. Chem. C* **2016**, *120*, 21047–21055. [[CrossRef](#)] [[PubMed](#)]
55. Ngo, H.T.; Wang, H.-N.; Fales, A.M.; Vo-Dinh, T. Label-Free DNA Biosensor Based on SERS Molecular Sentinel on Nanowave Chip. *Anal. Chem.* **2013**, *85*, 6378–6383. [[CrossRef](#)] [[PubMed](#)]
56. Ngo, H.T.; Wang, H.-N.; Fales, A.M.; Nicholson, B.P.; Woods, C.W.; Vo-Dinh, T. DNA bioassay-on-chip using SERS detection for dengue diagnosis. *Analyst* **2014**, *139*, 5655–5659. [[CrossRef](#)] [[PubMed](#)]
57. Ngo, H.T.; Wang, H.-N.; Fales, A.M.; Vo-Dinh, T. Plasmonic SERS biosensing nanochips for DNA detection. *Anal. Bioanal. Chem.* **2016**, *408*, 1773–1781. [[CrossRef](#)] [[PubMed](#)]
58. Wang, H.-N.; Register, J.K.; Fales, A.M.; Gandra, N.; Cho, E.H.; Boico, A.; Palmer, G.M.; Klitzman, B.; Vo-Dinh, T. Surface-enhanced Raman scattering nanosensors for in vivo detection of nucleic acid targets in a large animal model. *Nano Res.* **2018**, in press. [[CrossRef](#)]
59. Wang, J.-W.; Czech, B.; Weigel, D. miR156-Regulated SPL Transcription Factors Define an Endogenous Flowering Pathway in Arabidopsis thaliana. *Cell* **2009**, *138*, 738–749. [[CrossRef](#)] [[PubMed](#)]

